

Realtime Atmospheric Decision Aids in Support of the Lunar Laser Communications Demonstration

Randall J. Alliss and Billy Felton
Northrop Grumman Corporation
7555 Colshire Drive
McLean, Virginia 22102
Randall.alliss@ngc.com

Abstract— Atmospherics, in particular clouds, are a key driver in the performance of free space optical communication (FSOC) systems. Clouds are composed of liquid water and/or ice crystals, and depending on the physical thickness, can produce atmospheric fades easily exceeding 10 decibels (dB). In these more common cases, impacts on FSOC systems may be severe. On the other hand, there are times when cloud fades may be as low as 1 or 2 dB as a result of thin, ice crystal based cirrus clouds. In these cases, the impacts on FSOC communication collectors may be limited.

The ability to characterize the distribution and frequency of clouds is critical in order to understand and predict atmospheric impacts on FSOC. A realtime cloud analysis and forecasting system has been developed to support the Lunar Laser Communications Demonstration (LLCD). LLCD will demonstrate high data rate optical communications from lunar orbit to three ground sites. The realtime cloud analysis and forecasting system supporting LLCD is composed of remotely sensed clouds derived from geostationary meteorological satellites from the United States Geostationary Operational Environmental Satellite (GOES) and the Meteosat Second Generation (MSG) Severi instrument. Cloud analyses are derived from these satellites for three ground sites: White Sands Complex (WSC), New Mexico, the primary ground site for LLCD; Table Mountain Facility (TMF) in Southern California; and Tenerife Optical Ground Station (OGS) in the Canary Islands. Analyses are derived every 15 minutes at 1-kilometer horizontal resolution. Using these cloud analyses, a Cloud Free Line of Sight (CFLOS) indicator is computed from each site to the current moon position and provided in realtime to mission planners. In addition to the current CFLOS, a short term cloud forecast is derived based on recent motion of clouds around each site. These forecasts are being used for planning purposes to decide which site is most desirable for optical communications during LLCD's next pass around the moon. In addition, a cloud forecast out to 16 days is being used for longer term mission planning. These forecasts are derived from numerical weather prediction models of the atmosphere.

The goal of this capability is to determine the feasibility of using realtime atmospheric products for the mitigation of the effects of clouds on FSOC. The LLCD project gives us the opportunity to quantitatively assess how such products perform so that future space to ground applications, including

handover between ground sites, may take advantage of the experience gained. This presentation will show results from the analysis of the forecasting system generated during LLCD.

Keywords: *optical communications, lasercom, clouds, availability.*

I. INTRODUCTION

Strategies to support high-availability laser communications for future missions from space to Earth are increasingly receiving attention. Such missions will generate an ever increasing amount of data that must be transferred to ground locations on Earth. As an alternative to the current use of radio communications, deep space to ground optical communications will provide a higher bandwidth to transfer these data with smaller power mass and power consumption subsystems. However, optical communications may be interrupted by the presence of cloud cover. Typical clouds have optical fades that far exceed three dB. Therefore, it may not be feasible to include enough link margin in the link budget to prevent a link outage. It should be noted that some cirrus clouds may have optical fades less than three dB when averaged over many minutes (Figure 1). However, an optical communications link directed through the sky may encounter "knots" or areas within thin cirrus that may far exceed three dB. Therefore, a mitigation strategy ensuring a high likelihood of a cloud-free line of sight (CFLOS) between a ground station and the spacecraft is needed to maximize the transfer of data and overall availability of the network.

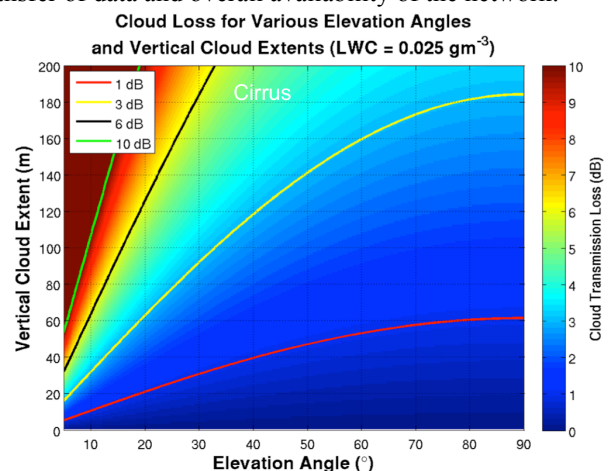


Figure 1. Transmission loss due to a typical cirrus cloud as a function of elevation angle and cloud thickness.

The Lunar Laser Communications Demonstration (LLCD) was launched on board the Lunar Atmospheric Dust Environment Experiment (LADEE) from Wallops Island, Virginia in early September 2013 (Figure 2). The goal of this experiment was due to demonstrate the first ever moon orbit to earth station optical communications.



Figure 2. Stage one and two of the LADEE launch from Wallops Island, Virginia.

The LLCD took place between approximately mid October and mid November of 2013. The purpose of this study was to use remote based cloud detection from satellite to monitor the three LLCD sites in near realtime. These sites included White Sands (WSC), NM, Table Mountain Facility (TMF), and Optical Ground Station (OGS) on Tenerife in the Canary Islands. The remotely sensed clouds are a proxy for ground based cloud detection which is highly desired for ground stations in general because they would provide higher temporal and spatial resolution cloud information in order to make decisions on the suitability of the site. In addition to the satellite derived cloud detection and algorithm has been developed to predict the location of clouds up to two hours into the future based on recent cloud motion.

Section two, describes the satellite based cloud detection algorithm, section three provides an overview of the short term cloud forecasting algorithm and section four shows examples and results to date.

II. CLOUD MASK GENERATOR

A. Satellite Data

The satellite derived cloud analysis is derived from two satellites. These are the Geostationary Operational Environmental Satellite (GOES)-13 which covers the WSC and TMF ground sites and the Meteosat Second Generation (MSG), which covers OGS in the Canary Islands.

GOES imagers have five bands: visible (0.6 μm), shortwave infrared (SWIR; 3.9 μm), water vapor (6.7 μm), longwave infrared (LWIR; 10.7 μm), and CO₂ channel (13.0 μm). We

replaced the water vapor channel, which is not used for cloud detection, with the reflectivity product during the day and the fog product at night. The spatial resolution of the visible band is 1 km and that for the other bands is 4 km. For our purposes, the 4 km data is resampled to 1 km resolution so that it is comparable to the visible band. GOES imagery is available every 15 minutes. The MSG satellite has similar bands and the data is also utilized at 1km resolution. MSG data is also available at 15 minute temporal resolution.

B. CMG Algorithm

Our cloud analysis techniques for the GOES data are described in detail by Alliss et al.¹. All cloud tests consist of comparing satellite image values to dynamically computed clear sky background (CSB) values pixel by pixel in the regions of interest. The CSB is discussed below and main cloud test algorithms (albedo, LWIR, fog, and reflectivity) are discussed in section 2.3.

The CSB is defined as the amount of radiation emitted and/or reflected from a surface that reaches a satellite sensor when no clouds are present. The CSB varies spatially and temporally and is influenced by the radiative properties of the surface material, surface temperature, terrain height, soil moisture, and solar illumination angle. Because of these variations, the CSB must be calculated for each region separately, on a pixel by pixel basis, as a function of the above-mentioned factors to generate accurate cloud masks. For example, if the albedo test used a fixed threshold for typical differences between the observed and calculated CSB albedos for all locations, then false cloud detections would be likely over naturally highly reflective regions such as White Sands, NM or the salt flats of northern Chile.

Four CSBs are estimated in the CMG: albedo, reflectivity, LWIR, and fog¹. The CSB is calculated for each pixel by using data from clear times over the previous 30 days at a given analysis time (e.g., 1400 GMT). This approach provides sufficient clear sky data and reduces the effect of diurnal and seasonal cycles of temperature and illumination, in particular, on the calculated CSB. The database from which clear times are determined includes not only the satellite imagery, but also ancillary surface and ship observations collected by the National Weather Service (NWS), World Meteorological Organization (WMO), and at several telescope observatories in South America.

The albedo CSB is calculated by identifying the darkest 10 % of albedo values from the previous 30 days of visible images. The selected albedo values are averaged to define the CSB for each pixel. The reflectivity CSB is determined only during the day and when snow cover is not likely present. Like the albedo, the darkest 10 % reflectivity product values from the previous 30 days are selected and averaged to generate the CSB.

To develop the fog product CSB, the warmest 10 % of LWIR values for the pixel over the previous 30 days are selected.

The corresponding fog product values are then averaged to give the fog CSB. Note that the procedure used to generate the fog product CSB differs from that used to generate the albedo and reflectivity products in which clear pixels are chosen based on the albedo and reflectivity values themselves. Both fog product extremes indicate clouds and the selection of the 10 % warmest or coldest values will not provide the needed information; therefore, the two-step process is used for the fog product CSB.

The LWIR CSB is determined as the average of the difference between the LWIR temperature from the satellite for a given pixel and the LWIR CSB temperature estimated from a linear regression model. The regression model is developed with data from clear sky pixels that are used as prototypes. These prototype pixels are selected by a series of tests that find pixels with a high probability of being clear, even without the benefit of any of the cloud tests. The coefficients of the regression model for twelve predictors are fit with the data from the prototype pixels. The predictors include satellite data, time, terrain, and regional observations such as cloud cover and air temperature from the NWS and WMO. The LWIR regression model estimates the clear sky LWIR brightness temperature for each pixel. The LWIR residuals are the differences between the regression model temperatures and the measured imager LWIR temperatures. The warmest 10 % of the LWIR residuals are averaged to determine the LWIR residual CSB that is used in the LWIR cloud tests.

C. Cloud Tests

The CSB values and the satellite data are compared in four main cloud tests in the CMG: the LWIR test, the albedo product test, the fog product test, and the reflectivity product test. The LWIR test is applied at all times of the day, unlike the albedo, reflectivity, or fog product tests. A pixel is considered to be cloudy if the LWIR CSB for a given pixel exceeds the LWIR from the satellite by the threshold value or greater. This test cannot easily detect fog/low clouds at night because the cloud top temperatures are very similar to the surface temperatures. It is unlikely that clouds will radiate in the LWIR at temperatures greater than 300K. A pixel is deemed clear if the LWIR temperature is greater than 300K, even if the LWIR cloud test indicates that it is cloudy.

As mentioned above, the detection of fog and low stratus clouds at night is difficult with the LWIR. The fog product test is a multi-spectral test that compares values of the fog product calculated as the difference between the LWIR and the SWIR brightness temperatures^{2,3,4}. The temperature differences result mainly because clouds observed in the SWIR have an emissivity that is 20%-40% lower than clouds observed in the LWIR⁵. Therefore, at night, liquid stratiform (low) clouds appear colder in the SWIR than they do in the LWIR. Typical $T_{LWIR} - T_{SWIR}$ for fog and low stratus are approximately 2 K or larger⁶. The fog product can also detect ice clouds, which are highly transmissive and therefore appear warmer in the SWIR. Typical values for ice clouds are $T_{LWIR} -$

T_{SWIR} are approximately -5 K or lower⁶. The daytime SWIR is dominated by reflected solar SWIR and therefore, the fog product is only useful at night.

The albedo test, which uses visible data, is applied when the solar zenith angle is below 89°. This test will detect clouds if the pixel is more reflective than the albedo CSB and the difference is greater than a predefined threshold for that pixel. If the difference between the calculated albedo and the CSB is less than the threshold, the pixel is deemed clear. The albedo test may falsely detect snow as clouds.

The shortwave reflectivity product is implemented during the day to decide if a pixel is cloudy or if the surface is snow-covered. This product indicates the amount of reflected solar SWIR detected and is derived by removing the thermal component from the SWIR^{5,6}. Water clouds are highly reflective in the SWIR while ice clouds are poorly reflective in the SWIR. As a result, water clouds appear as bright white and poorly reflective ice clouds and snow appear as dark gray or black in the resulting images. The reflectivity product, then, can easily distinguish between low clouds and snow cover. The reflectivity test is only applied when and where snow cover is likely and can override a false cloud detection for snow cover indicated by the albedo test. To ensure that high ice clouds (which also appear dark in the reflectivity test) are not present, the LWIR test must not indicate the presence of high clouds for a pixel to be considered clear.

With the CSB and satellite data, the CMG performs the multispectral tests to accurately distinguish between clouds and clear skies. During the day, for example over southern the Canary Islands (Figure 3), the LWIR and albedo products are used to detect clouds with the resulting mask accurately showing the presence of clouds around the summit of Tenerife. At night when low clouds cannot be adequately detected by the LWIR, the fog product is vital to developing accurate cloud masks. A cloud scene from Hawaii (Figure 4), the low clouds over the land would not have been detected without the fog product.

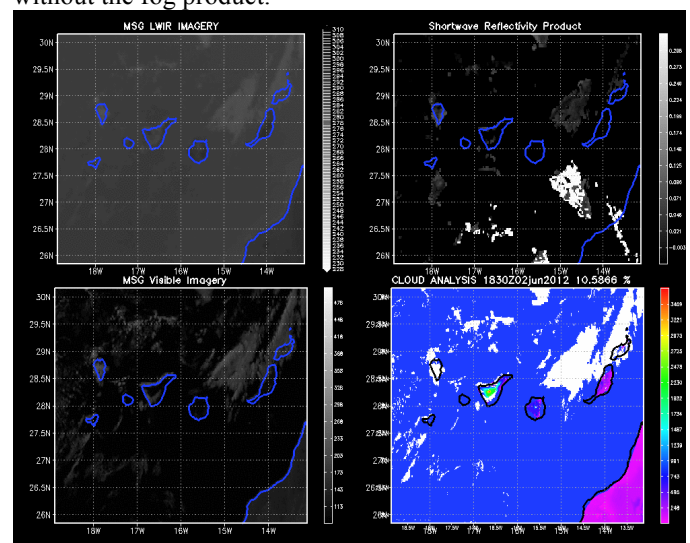


Figure 3: A sample cloud scene during the day for the Canary Islands. The image on the upper left is the LWIR image from MSG during the day. The image in the upper right is the reflectivity product, the lower right shows the 1km visible channel and the lower left shows the resulting composite cloud analysis.

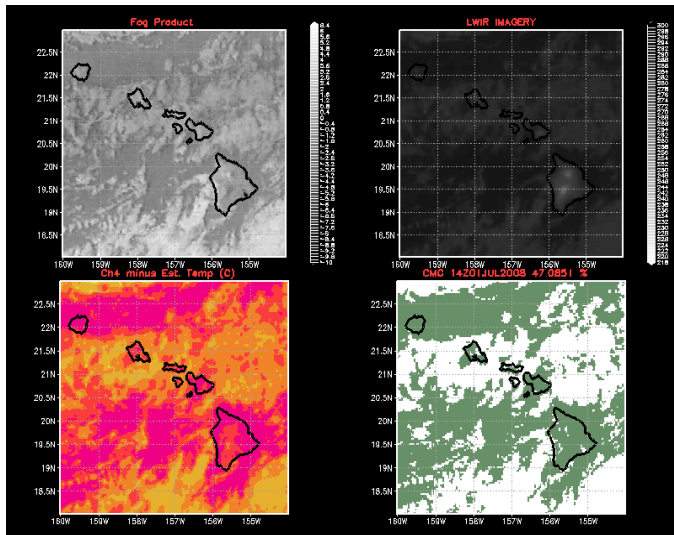


Figure 4. Fog Product (upper right), LWIR imagery (upper left), longwave infrared modeling (lower left), and composite cloud test (lower right) of a nighttime scene over Hawaii.

III. CLOUD PROPAGATOR FORECAST (CPF)

The CPF operates on successive cloud masks to produce reliable probability forecasts of future cloud cover conditions at each point location (single mask grid cell) or for the expectation of the amount of sky cover in a local skydome about each point location. This discussion covers the point probability mode, with exceptions for skydome mode presented at the conclusion.

The CPF makes reads CMG gridded data, from either the historical or real time-modes, and produces a single forecast time slice valid a specified time in the future. The output from the CPF is placed into identically formatted output files, with forecast fields stored in the time positions equal to the valid times of the forecasts. The CPF retains trained model data from previous runs for the same tile, and is capable of bootstrapping itself rapidly if no prior run model data are available.

The forecasting algorithm is a combination of empirical Lagrangian and Eulerian regression over multiple spatial scales, but treats time auto-regressively. Input cloud masks are transformed into proxies first. A cloud cover proxy is a variable which has a more Gaussian distribution than literal cloud cover. For a given pixel, the cloud cover proxy is computed first by determining whether at the initialization time the pixel was clear or cloudy. Clear pixels will be

assigned only positive proxies; cloudy pixels will be given only negative proxies. The degree the assigned proxy is different than zero depends on the fraction of pixels in a small neighboring space that have similar cloudy/clearness. The neighboring space is approximately the spatial scale of a skydome and has a temporal scale of one hour. Pixels which are unlike their neighbors will have proxies close to zero, those largely identical to their neighbors will have proxies close to plus or minus one. Final cloud proxies are computed using a non-linear transform to stretch out the extremes into a pseudo-Gaussian distribution.

The model then decomposes the proxy fields into scale-filtered components. Longer spatial scale patterns are expected to be more predictable over time; shorter scales less so. Differentiating them allows the model to retain the maximum predictive skill through training. The training is performed in pure-hindsight. A hindsight forecast is constructed from past data and is evaluated against current proxies to update motion vectors and regression weights. Motion vectors are computed on each scale using a fast local search which maximizes offset spatial pattern correlations. The motion vectors are an exponentially deweighted running mean. Regression predictors are extracted from the predictor field centered at the motion vector offset, with a 3x3 or 5x5 array (configurable) of samples taken spaced at the characteristic length of the spatial component. The prior regression models are deweighted exponentially, similarly to the motion vectors, so that evolving weather patterns can be followed rapidly by the modeling. The regression models produce minimum error estimates of the current time proxy, as a function of a proxy offset from the past. If multiple forecast lead times are configured for the run, then multiple motion/regression models are independently used.

Additionally, the hindsight proxy forecasts to the initialization time are tracked in concert with actual cloud/no-cloud statuses of the hindsight training data. These are accumulated in reliability tables which have separate slots for eight three-hourly times of day to allow forecast accuracy to be diurnally variable. These tables are also exponentially deweighted, but with a time-scale over days rather than hours. Finally, training is not executed for time steps where input data quality is thought to be low. This decision is made by examining the absolute change in regional cloud cover over a single time step and comparing it to a user configurable threshold. The motion/regression models are saved, and then the model is run from the current time, forward, to create a future proxy forecast. The proxies are translated into cloud cover by interpolated look-up into the reliability tables. The results are shown as probabilities of cloud at each pixel in the forecast image. A high level schematic is shown in Figure 5 which outlines the CPF generation.

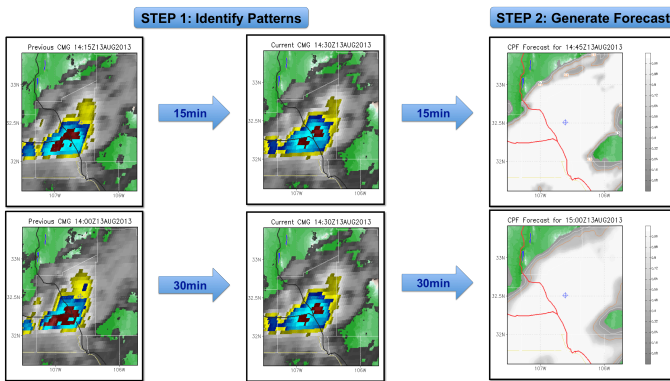


Figure 5. CPF is generated by analyzing sequential images of clouds derived from the CMG. Patterns of motion are established and a forecast for future locations are generated.

IV. RESULTS

A. Decision Aids for Mission Operations

The Objective of this research was to develop a variety of atmospheric decision aids to characterize the approximate line of sight to LLCD. Specifically, the objectives were to 1), Provide forecasts of the probability that clouds will block LLCD transmission to each LLCD ground station, 2) provide short-range forecasts out to two hours based upon recent cloud motion derived from satellite imagery from GOES and MSG satellites, 3) provide Mid- and longer- range forecasts, out to 3.5, 5, and 16 days, computed from numerical weather prediction (NWP) ensemble forecasts, and, 4) provide forecasts of optical turbulence properties from NWP.

Short range cloud forecasts are updated every 15 minutes. The Cloud Propagator Forecast (CPF) uses cloud analyses from the most recent several satellite images to compute cloud motion vectors. These are used to forecast the probability of cloud at each grid point in the domain every 15 minutes out to two hours. The figure 5 above gives an example of such a forecast.

Mid-range forecasts for LLCD were generated from the Short Range Ensemble Forecast (SREF) and Global Ensemble Forecast System (GENS) ensemble forecasts, and were updated every six hours. The SREF and GENS data were downloaded from the National Center for Environmental Prediction (NCEP) in the U.S. four times daily, and the total cloud amount parameters were extracted from the datasets. The probability that the cloud amount exceeded the threshold was computed from the 21 ensemble members' cloud amounts for each forecast time. Decision aids based upon the forecast cloud amounts were created and updated on the LLCD website each time new data was available. SREF forecasts were available every three hours out to 87 hours, covering North America and the eastern Pacific and western Atlantic oceans. GENS was used to forecast clouds for operational purposes out to five days, and to provide general guidance out to 16 days. Products were similar to the mid-range products, and included go/no-go decisions, forecast cloud amount

distributions from the ensemble members, and cloud forecast map animations. Decision aids were shown as a function of forecast lead time.

Quick-look decision aids were developed to provide mission operators go/no-go guidance. Stoplight plot shows the probability of cloud-free operation (green, yellow, red) as well as whether the moon is below the horizon (X). Figures 6 shows an example of the current cloud conditions at each site as well as the most recent 12 hours. This product was updated every fifteen minutes as new satellite imagery was ingested and processed into the cloud mask. The stop light shows whether the line of site to LLCD was clear (Green) or cloudy (Red). The graph indicates the approximate sky cloud fraction over the last twelve hours and the stop light at the bottom shows whether the LOS was clear/cloudy over the last twelve hours. It's important to point out that the indication of the line of site is only an approximation since the depth of the cloud is not known from satellite. Therefore any clouds in the line of site to LLCD whether it was actually above/below the line of site is assumed to block the signal.

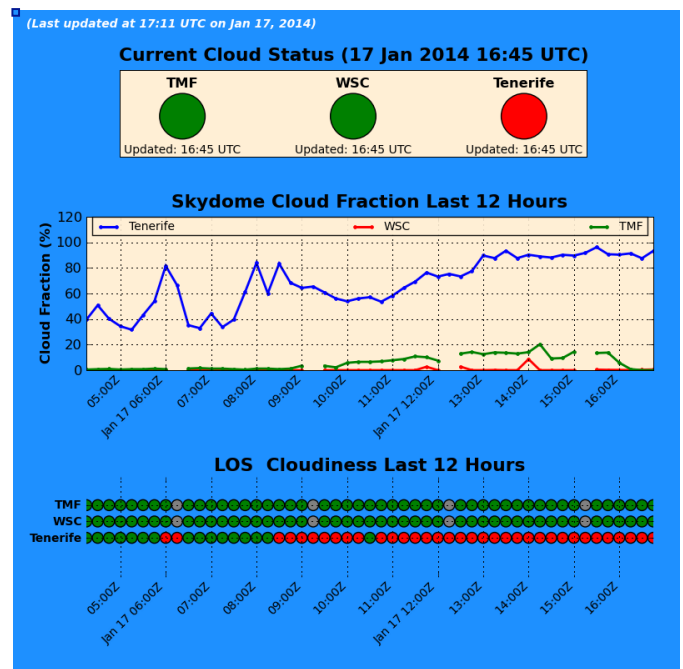


Figure 6. Current and recent cloud conditions at each site. Green light indicates mainly clear skies and red light indicates clouds greater than 30%.

The short-term, two hour, cloud forecast derived from the CPF is shown in Figure 7. Each row in the figure shows the anticipated skydome cloud fraction at each site in fifteen minute intervals out to two hours. Clear skies, less than 30% cloud fraction is shown in green, marginal, defined as skydome cloud fraction between 30-50% is shown by a yellow light and greater than 50% is shown by a red light. When LLCD was expected below the horizon a large X was overlaid on the stop light. In some cases the stop light may have

concentric rings overlaid. In these cases LLCD was above the horizon but had an elevation angle less than 15 degrees.

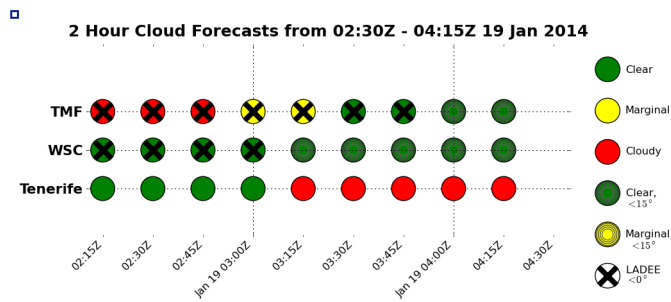


Figure 7. Two Hour cloud forecast of line of site derived from the CPF.

In order to give missions planners longer leadtime to prepare for upcoming passes a twenty four hour cloud forecast was generated for each site (Figure 8). The legend used is identical to that of the two hour forecast. This product was updated every six hours as new model data became available. The test director was able to use this product in order to determine if the primary site (WSC) would be useable or not. Note there were times when all three sites had access to LLCD although this was limited to just a pass or two per day.

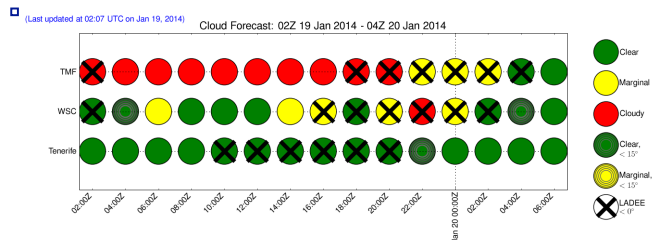


Figure 8. Twenty hour forecast derived from the SREF and GENS at two hourly increments.

LLCD was composed of four separate operational periods consisting of four days on followed by three days off. Each block lasted approximately one week. In order to have some idea of what the weather would be like for future blocks an extended range cloud product was produced (Figure 9). Figure 9 shows a sixteen day cloud forecast derived from the NCEP GENS ensemble system. This product was not intended to serve as a proxy for the actual line of site but rather a broad indicator of the likely hood of clouds in and near each site. In many cases this product would show how the WSC and TMF sites were much more correlated in clouds than with the Tenerife site. However, there was often a temporal lag in the expected cloud cover between TMF and WSC, usually by just a day or two. Operators would be able to use this product to gaze up to two blocks into the future. However, guidance at these long ranges often contained a high degree of uncertainty and therefore had to be used as only a top level first guess at the future. This data was also provided in the form of a series of forecast maps of clouds (Figure 10).

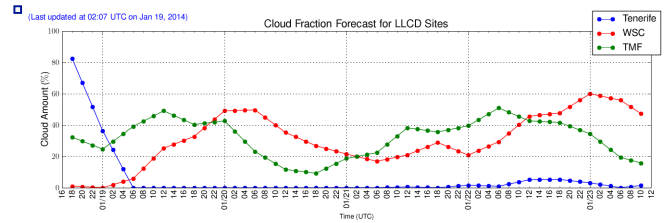


Figure 9. Long range guidance on expected cloud fraction for each site.

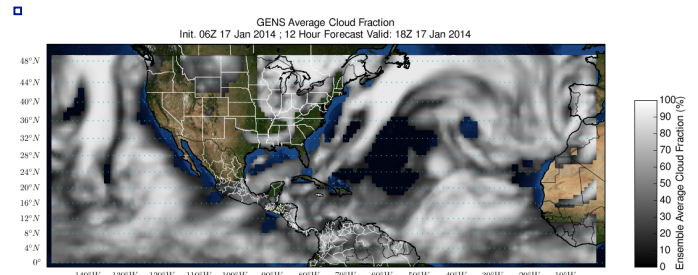


Figure 10. Forecast map of clouds derived from the GENS showing cloud predictions for all three sites simultaneously.

B. Results during LLCD Operations

At the time of this writing only the CPF forecasts were available for comparison to the CMG. Table 1 below shows the root mean square errors (RMSE) and bias of the CPF versus CMG. The data is sorted by forecast length from 15 minutes to 120 minutes. Results are only shown for “power on times”, MIT personal communication. The power on times represents those times when the space terminal was transmitting to the LLGT or TMF sites. All the sample size is relatively small both the RMSE and bias are remarkably small. There is virtually no bias in either direction (over prediction or under prediction of clouds) relative to the CMG.

Forecast length (minutes)	RMSE (WSC)	Bias (WSC)	RMSE (TMF)	Bias (TMF)
15	0.10	-0.004	0.02	-0.020
30	0.17	0.001	0.04	-0.040
45	0.16	0.020	0.12	-0.050
60	0.17	-0.010	0.09	-0.030
75	0.21	-0.020	0.14	-0.060
90	0.23	-0.040	0.14	-0.070
105	0.23	-0.060	0.14	-0.070
120	0.24	-0.070	0.15	-0.080

Table 1. RMSE and Bias of CPF versus CMG at White Sands, NM and Table Mountain Facility (TMF).

V. SUMMARY AND CONCLUSIONS

A series of atmospheric decision aids were developed to support the characterization of three ground sites during the Lunar Laser Communications Demonstration. These decision

aids were based on remote sensed data from the GOES and MSG satellites as well as numerical weather prediction forecasts of clouds. The decision aids were used to characterize the current cloud conditions at each site as well as provide guidance on the anticipated cloudiness over the next orbital pass (2 hours). In addition longer term guidance was developed to predict whether the sites would be cloud free from a few days out to as many as 16 days. Results indicate that the very short term forecasts were far superior to the long range guidance as expected. Decision aids for the future will be based on *insitu* data collected at optical ground sites. Examples of this include visible and infrared based whole sky imagery.

REFERENCES

- [1] R. J. Alliss, M. E. Loftus, D. Apling, and J. Lefever, "The development of cloud retrieval algorithms applied to goes digital data," in *10th Conference on Satellite Meteorology and Oceanography*, pp. 330–333, American Meteorological Soc., January 2000.
- [2] G. P. Ellrod, "Advances in the detection and analysis of fog at night using goes multispectral infrared imagery," *Weather Forecasting*, **10**, pp. 606–619, 1995.
- [3] G. E. Hunt, Radiative properties of terrestrial clouds at visible and infrared thermal window wavelengths," *Quarterly Journal of the Royal Meteorological Society*, **99**, 346-359.
- [4] T. F. Lee, F. J. Turk, and K. Richardson, "Stratus and fog products using GOES-8 3.9 μm data," *Weather Forecasting*, **12**, pp. 664–677, 1997.
- [5] R. C. Allen, Jr., P. A. Durkee, and C. H. Wash, "Snow/cloud discrimination with multispectral satellite measurements," *Journal of Applied Meteorology*, **29**, pp. 994–1004, 1990.
- [6] M. Setvak and C. A. Doswell, III, "The AVHRR channel 3 cloud top reflectivity of convective storms," *Monthly Weather Review*, 119, pp. 841–847, 1991.